Dynamics of soil pore space structure investigated by X-ray microtomography

Stephan Peth[A], Jens Nellesen[B], Gottfried Fischer[C], Felix Beckmann[D] and Rainer Horn[A]

[A]Institute of Plant Nutrition and Soil Science, Christian-Albrechts-University zu Kiel, Germany
[B]Lehrstuhl für Qualitätswesen, Department of Mechanical Engineering, Technische Universität Dortmund, Germany
[C]Dortmunder Initiative zur rechnerintegrierten Fertigung (RIF) e.V., Joseph-von-Fraunhofer-Str. 20, D-44227 Dortmund, Germany
[D]GKSS Research Centre, Hamburger Synchrotron-Strahlungslabor, Deutsches Elektronensynchrotron, Hamburg, Germany

Abstract
Transport and transformation processes of solid, liquid and gaseous compounds/components in soils are intimately connected and strongly dependent on the state of soil structure and pore space geometries. Soil structure in turn is inherently dynamic due to changes in pore water pressure resulting in shrinking and swelling and/or soil compaction and shear deformation by applying external loads and last but not least also continuously modified by biological factors (root growth and soil faunal activities). Studying the dynamic properties of soils and functions requires observing the evolution of soil structure with changing boundary conditions without disturbing the processes of structure formation. Non-invasive techniques such as X-ray microtomography are able to resolve soil structure and associated pore architectures on various scales and at the same time allow for non-destructive observations of structural dynamics upon changes in boundary conditions. We used synchrotron- and X-ray microfocus tube-based microtomography (SR-µCT and MF-µCT resp.) systems to investigate soil structural dynamics of soil aggregates and typical core-size soil samples. The effects of shrinking/swelling and compaction on pore space architectures were studied under controlled boundary conditions (matric potential, mechanical loads). Three-dimensional reconstructions of the pore space were analyzed with 3D image analysis tools to quantify changes in morphological characteristics of soil structure and related pore networks upon changes in boundary conditions, respectively. The potential of such quantitative data to further develop modeling approaches of transport and deformation processes in soils will be discussed. Further improvements in µCT imaging approaches and 3D image analysis of soil structure dynamics coupled with physical measurements of transport functions are essential to achieve a more comprehensive understanding of soil-ecosystem fluxes and interactions.

Key words
X-ray microtomography, image analysis, 3D correlation analysis, soil mechanics, soil deformation, soil structure.

Introduction

Non-invasive three dimensional imaging microscopy using microtomography techniques provide a useful method to directly observe and quantify soil structure formation and deformation with changes in hydraulic and mechanical stress state. The advantage over other imaging techniques applied in soil morphology analysis (e.g. thin sectioning) is that tomography measurements account for the 3D nature of the specimen and that samples remain intact after CT image acquisition measurement allowing for repeated imaging and thus monitoring soil structure dynamics. The latter is a prerequisite to observe spatial modifications of the soil pore microenvironment caused by dynamic processes continuously re-arranging pore networks hence feeding back on soil functions. On the other hand, indirect assessments of soil structural attributes such as the pore size distribution (PSD) derived from water retention curves (WRC) render inaccurately in a sense that with changes in hydraulic stress during the measurement pore geometries may change resulting in a continuously modified pore size distribution during the course of the measurement. The same is true for the derivation of hydraulic model parameters from such indirect measurement methods since the non-rigidity of pore systems caused by shrinking–swelling processes is not considered. Non-invasive imaging techniques could overcome some of the limitations of routinely applied methods for assessing soil structure and associated soil functions.

Methods

We used two sets of samples for this study:
Firstly, a soil aggregate sample (~5 mm across) was collected from an *Alfisol* (Rotthalmünster, Germany) from the topsoil layer. The soil aggregate sample was scanned in air dry condition at the synchrotron microtomography facility operated by the GKSS Research Center at HASYLAB (Hamburger Synchrotron Strahlungslabor) of DESY (Deutsches Elektronen Synchrotron) in Hamburg/Germany. The microtomography was completed at beamline BW2. The sample was mounted on a rotary stage and scanned

at a photon energy of 24 keV and a voxel resolution (voxel edge length) of 4.38 µm. During the microtomographical scan the sample was rotated at different projection angles between 0 and π, at 0.5° degree intervals. The absorption radiographs for the different viewing angles were projected onto a $CdWO_4$ fluorescent screen and recorded by a 1536×1024 pixel CCD camera. Image reconstruction was accomplished using a filtered back-projection algorithm in IDL™ (Research Systems Inc.). Attenuation coefficients are expressed as grayscale values ranging from [255] for the highest attenuation coefficient to [0] for the lowest attenuation coefficient reached. After the initial scan the sample was wetted via a glass fibre wick from below at a suction of -7 hPa with a 1M KI-doped solution to increase the attenuation contrast of the fluid phase. After imbibition the same aggregate was scanned a second time.

In a second series bulk soil samples have been prepared in the laboratory. Remoulded loess soil material has been filled into 5 cm diameter *Plexiglas® cylinders* at three different initial bulk densities (1.00, 1.20 and 1.33 g/cm^3, respectively). Samples were scanned at three different conditions: 1) initial homogeneous condition, 2) after saturation and 3) after subsequent air drying. Following the investigation of shrinking/swelling effects on soil structure development we studied the response of the structured soil to mechanical stresses. To do this we applied stepwise increasing mechanical loads of up to 400 kPa to the dried sample with the intermediate packing density (1.20 g/cm^3) in air dry condition. For the loading steps of 0, 20, 50, 100, 200, and 400 kPa we tomographed the sample immediately after loading.

The above mentioned remoulded soil samples were scanned in a lab by a *phoenix v|tome|x | 240* (GE Sensing & Inspection Technologies GmbH, Wunstorf, Germany). Scanning procedure is similar to the procedure done at the HASYLAB except that a polychromatic and cone shaped X-ray beam is used instead of a monochromatic parallelized beam as it is generated at synchrotron facilities. X-ray parameters used were 200 keV scanning energy with 1440 projections per sample with a voxel resolution between 38.4 and 41.0 µm. The basic setup of the scanning system and image processing is shown in Figure 1.

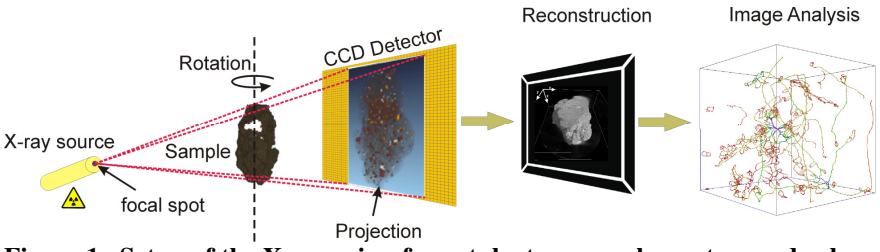

Figure 1. Setup of the X-ray microfocus tube tomography system and subsequent image reconstruction and analysis.

Volume rendering of the image reconstructions has been carried out with VG-Studio Max 2.0 (Volume Graphics GmbH, Heidelberg, Germany). Morphological image analysis of the grayscale images has been performed with a suite of algorithms assembled in the software package *3dma-Rock* (Lindquist *et al.* 2005) and in VG-Studio Max 2.0. A full 3D image analysis consists of a succession of image transformations and ends with the quantification of pore network characteristics (Figure 2). Basic image transformations are *segmentation*, *disconnected cluster clean up*, *medial axis construction* and *throat and pore size computation*. An analysis of strain localisation was performed by digital 3D tomogram correlation after Crostack *et al.* (2008). A reference tomogram was divided into cuboid regions which are regularly distributed on a regular grid. Each cuboid represents the local microstructure in the reference state (before shrinking or loading) at its grid point. The cuboids in the reference tomogram are iteratively mapped onto the corresponding more or less deformed microstructural parallelepiped-shaped region in the comparison tomogram (after shrinking or loading). By coordinate transformations a mean deformation gradient F and the Lagrangian strain tensor γ are derived and from this scalar deformation quantities like volume change dV/V and equivalent strain ε_{equ} can be calculated. Further details on the method and its application for the determination of localized soil deformation using microtomography images are provided in Peth *et al.* (2010).

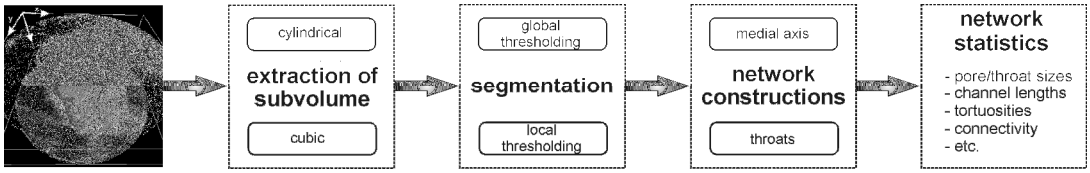

Figure 2. Basic image transformation steps in *3dma-Rock*.

Results

The effect of a change in hydraulic stress on pore geometry is demonstrated in Figure 3 where the tomograms of a soil aggregate scanned in air dry condition and after imbibition of a 1M KI-solution at -7hPa are compared. After imbibition a rearrangement of particles accompanied by a restructuring of the pore space was observed. This is apparent from closing coarse, soil structure related pores (e.g. cracks) and interestingly also from the formation of new coarse pores that remain gas filled. Swelling is a common process in clay rich soils and well known to partially close previously generated cracks. In contrast the formation of new coarse pores during wetting is a phenomenon that has to the best of our knowledge not yet been observed directly. An explanation could be microscale gas flow processes leading to a local entrapment of air within the aggregate and subsequent deformation of the soil matrix as air pressure exceeds local soil strength (Peth *et al.* 2008b). Another reason could be contractile forces during capillary wetting of the previously air dry sample leading to the generation of new or a widening of pre-existing cracks. These observations underline the complexity of interactive transport and deformation mechanisms resulting in dynamic soil pore spaces pointing out that the investigation of pore scale processes requires non-invasive techniques.

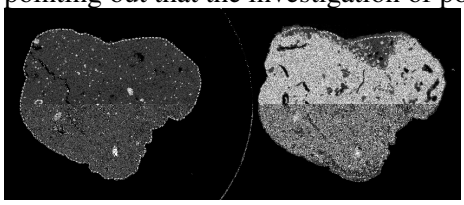

Figure 3. Tomograms before (left) and after (right) imbibition with 1M KI-solution at a matric potential of -7 hPa. The dashed line indicates the rim of the air dry sample before the sample was wetted. (taken from Peth 2010)

Development of soil structure in bulk soil samples is shown in Figure 4 exemplarily for the loose packing (1.00 g/cm^3) for the three conditions (initially dry homogenous, after saturation and after subsequent air drying). We observed almost no macropores in the initially homogeneous dry condition as it is shown more clearly in the binarized images in the bottom part of Figure 4. After saturation a substantial number of new macropores pores (> resolution limit which was approximately 40 µm) were generated indicated by the white areas in the binarized image. After drying the sample, again large cracks developed in the middle of the sample separating the bulk soil into five newly formed aggregates.

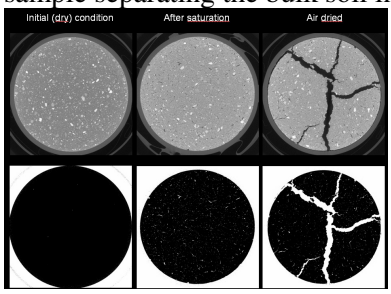

Figure 4. Tomograms (top) before (left) after saturation (middle) and after air drying (right). The binarized images (bottom) indicate the generation of new macropores by changes in hydraulic stresses (saturation and subsequent air drying).

Frequency distributions of pore size classes derived from morphological image analysis show that saturating the sample generated numerous macropores (Figure 5). Note that since close to the resolution limit (in this case ~ 40 µm) the detection of pores is associated with uncertainty due to binarization of the grayscale images only pores > 8 voxels (2 voxels wide in each spatial direction ➔ $2^3 = 8$) were counted to ensure that only real pores are included in the statistics. Interestingly subsequent shrinkage created a large crack, counted as one interconnected pore with a volume of 5.790 mm^3 (plotted at class < 10.000 mm^3 in Figure 5), but left the remainder pore size frequency distribution with pore volumes between > 0.0001 and < 1.000 mm^3 almost unchanged. Consequently, the pore volume gain within the newly formed crack must have been accommodated by pore volume reduction in pores smaller than 8 voxels in size corresponding to a volume equivalent diameter of spherical pores of < 50 µm.

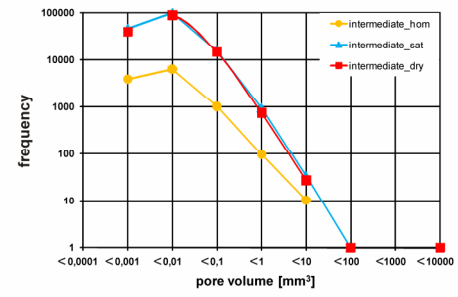

Figure 5. Frequency distribution of different pore size classes for the sample with intermediate packing density (1.20 g/cm^3; shown in Figure 4.) at three different conditions: initially homogenized = hom, saturated = sat, after shrinkage = dry).

Figure 6 presents the local soil deformation resulting from hydraulic (shrinkage, Figure 6A) and mechanical stresses (external loading, Figure 6B). The orientation of the major axis of the tensor ellipsoids (in this case represented as cuboids) in Figure 6A reveals a change in the orientation of the strain field from predominantly horizontal deformation at the outer rim of the sample to predominantly vertical deformation in the vicinity of the cracks in the centre of the sample during shrinkage. External mechanical loading of the sample in air dry condition resulted in spatially heterogeneous soil deformation (Figure 6B). We observed a strain concentration in the vicinity of larger cracks where plastic flow indicates a closure of the large cracks while within the interior of aggregates deformation is lower. A decreasing crack volume with mechanical loading was also determined by morphological image analysis (data not shown).

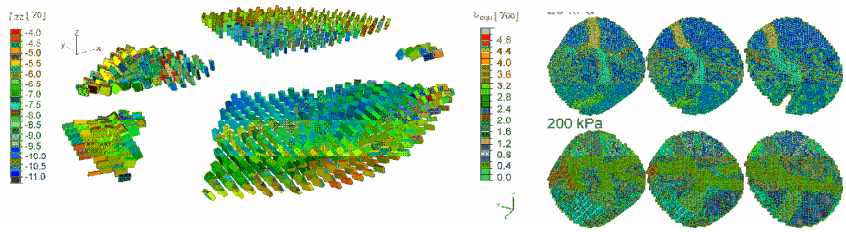

Figure 6. (A) Spatial orientation of the Lagrangrian strain tensor □ represented as cuboids for a tomogram correlation of the state before and after shrinkage showing the local magnitude of strain and the orientation of the maximum strain gradient. The slice represents a horizontal section near the top through the sample shown in B before mechanical loading. (B) Spatial distribution of the equivalent strain $\square_{equ}$ for two different external mechanical loads. The color scale is adjusted to lower strain values to indicate the deformation within the aggregates. The corresponding reference tomogram for the grayscale correlation analysis was in each case the unloaded state. Gray color coded areas indicate values of equivalent strain $\square_{equ}$ exceeding a specified threshold value (> 4.8 ‰) corresponding to a larger deformation in the vicinity of cracks.

Conclusion

Soil structure and associated pore space geometries are to be considered highly dynamic. Even in structurally mature units such as aggregates we observe modifications in the pore space by changing hydraulic stresses (imbibition). X-ray microtomography in conjunction with 3D image analysis techniques is capable to quantify the dynamic pore space in relation to changes of hydraulic and mechanical stress boundary conditions. The results presented here strongly suggest that soils are non-rigid systems where both hydraulic and mechanical stresses locally modify pore space geometries. These modifications are associated with a simultaneous destruction/reduction of pores/pore sizes and the generation of new pores. This fact has to be considered in modelling transport, deformation and exchange processes in soils and between the pedosphere and the atmosphere.

References

Crostack H-A, Nellesen J, Fischer G, Weber U, Schmauder S, Beckmann F (2008) 3D Analysis of MMC microstructures and deformation by µCT and FE simulations. In 'Developments in X-ray Tomography'. (Ed SR Stock). pp. 70781I1-12., VI, Vol. 7078 (SPIE, San Diego, CA).

Lindquist WB, Lee S-M, Oh W, Venkatarangan AB, Shin H, Prodanovic M (2005) 3DMA-Rock: A Software Package for Automated Analysis of Rock Pore Structure in 3-D Computed Microtomography Images. http://www.ams.sunysb.edu/~lindquis/3dma/3dma_rock/3dma_rock.html.

Peth S, Horn R, Beckmann F, Donath T, Fischer J, Smucker AJM (2008a) Three-Dimensional Quantification of Intra-Aggregate Pore-Space Features using Synchrotron-Radiation-Based Microtomography. *Soil Science Society of America Journal* **72,** 897-907.

Peth S, Horn R, Beckmann F, Donath T, Smucker AJM (2008b) The Interior of Soil Aggregates investigated by Synchrotron-Radiation-based Microtomography. In 'Developments in X-ray Tomography VI' (Ed SR Stock) pp. 70781H-12. (SPIE: San Diego, CA).

Peth S (2010) Applications of Microtomography in Soils and Sediments. In 'Synchrotron-Based Techniques in Soils and Sediments'. (Eds B Singh, M Gräfe) pp. 73-101.,Vol. 34. (Elsevier, Heidelberg).

Peth S, Nellesen J, Fischer G, Horn R (2010) Non-invasive 3D analysis of local soil deformation under mechanical and hydraulic stresses by µCT and digital image correlation. *Soil and Tillage Research*. (In press).